

# Computational Hemodynamics in Cerebral Aneurysms: The Effects of Modeled Versus Measured Boundary Conditions

ALBERTO MARZO,<sup>1</sup> PANKAJ SINGH,<sup>2</sup> IGNACIO LARRABIDE,<sup>3,4,5</sup> ALESSANDRO RADAELLI,<sup>6</sup> STUART COLEY,<sup>7</sup> MATT GWILLIAM,<sup>8</sup> IAIN D. WILKINSON,<sup>9</sup> PATRICIA LAWFORD,<sup>1</sup> PHILIPPE REYMOND,<sup>10</sup> UMANG PATEL,<sup>11</sup> ALEJANDRO FRANGI,<sup>3,4,5</sup> and D. ROD HOSE<sup>1</sup>

<sup>1</sup>Department of Cardiovascular Science, Academic Unit of Medical Physics, Faculty of Medicine and Biomedical Sciences, University of Sheffield, Beech Hill Road, S10 2RX Sheffield, UK; <sup>2</sup>Departments of Medical Physics and Neurosurgery, Royal Hallamshire Hospital, Sheffield, UK; <sup>3</sup>Centre for Computational Imaging and Simulation Technologies in Biomedicine, Universitat Pompeu Fabra (UPF), Barcelona, Spain; <sup>4</sup>Centre for Networked Biomedical Research on Bioengineering, Biomaterials and Nanomedicine (CIBER-BBN), Barcelona, Spain; <sup>5</sup>Institució Catalana de Recerca i Estudis Avançats (ICREA), Barcelona, Spain; <sup>6</sup>Philips Healthcare, Best, The Netherlands; <sup>7</sup>Department of Neuroradiology, Royal Hallamshire Hospital, Sheffield, UK; <sup>8</sup>Medical Physics and Clinical Engineering, Sheffield Teaching Hospitals NHS, Sheffield, UK; <sup>9</sup>Department of Human Metabolism, Academic Unit of Radiology, University of Sheffield, Sheffield, UK; <sup>10</sup>Laboratory of Hemodynamics and Cardiovascular Technology (LHCT), École Polytechnique Fédérale de Lausanne, Lausanne, Switzerland; and Department of Neurosurgery, Royal Hallamshire Hospital, Sheffield, UK

(Received 8 June 2010; accepted 9 October 2010; published online 23 October 2010)

Associate Editor Peter E. McHugh oversaw the review of this article.

**Abstract**—Modeling of flow in intracranial aneurysms (IAs) requires flow information at the model boundaries. In absence of patient-specific measurements, typical or modeled boundary conditions (BCs) are often used. This study investigates the effects of modeled versus patient-specific BCs on modeled hemodynamics within IAs. Computational fluid dynamics (CFD) models of five IAs were reconstructed from three-dimensional rotational angiography (3DRA). BCs were applied using in turn patient-specific phase-contrast-MR (pc-MR) measurements, a 1D-circulation model, and a physiologically coherent method based on local WSS at inlets. The Navier–Stokes equations were solved using the Ansys®-CFX™ software. Wall shear stress (WSS), oscillatory shear index (OSI), and other hemodynamic indices were computed. Differences in the values obtained with the three methods were analyzed using boxplot diagrams. Qualitative similarities were observed in the flow fields obtained with the three approaches. The quantitative comparison showed smaller discrepancies between pc-MR and 1D-model data, than those observed between pc-MR and WSS-scaled data. Discrepancies were reduced when indices were normalized to mean hemodynamic aneurysmal data. The strong similarities observed for the three BCs models suggest that vessel and aneurysm geometry have the strongest influence on aneurysmal hemodynamics. In absence of patient-specific BCs, a distributed circulation model may represent the best option when CFD is used for large cohort studies.

**Keywords**—Computational fluid dynamics, Phase-contrast MRI, 1D circulation model.

## INTRODUCTION

An aneurysm is a localized dilation in a blood vessel, which carries an inherent risk of rupture and consequent hemorrhage; for cerebral aneurysms rupture results in a subarachnoid hemorrhage (SAH). Despite improvements in surgical and medical management, SAH is still a major cause of morbidity and mortality.<sup>20</sup>

Although the etiology of the disease remains unclear, there is a growing consensus that hemodynamics plays an important role in the growth, rupture, and initiation of intracranial aneurysms (IAs).<sup>6,38,40</sup>

In this respect, a reliable prediction of stress or strain of the aneurysm wall would possibly offer a greater diagnostic capacity in the context of imminent rupture (it is likely that the event of rupture occurs when the tissue stress or strain exceeds some sustainable level). The stress and strain in the aneurysm can be calculated if the geometry, material characteristics, and boundary (support) conditions are known: unfortunately this will never be true for an individual and approximations would be required for all of them, thus compromising accuracy. The hemodynamic characterization returns parameters that might drive

Address correspondence to Alberto Marzo, Department of Cardiovascular Science, Academic Unit of Medical Physics, Faculty of Medicine and Biomedical Sciences, University of Sheffield, Beech Hill Road, S10 2RX Sheffield, UK. Electronic mail: a.marzo@shef.ac.uk, avmarzo@gmail.com

biological processes that are important in the evolution of an aneurysm toward a state in which it will rupture. This, despite a smaller diagnostic capacity might provide more accurate predictions, which might prove important with respect to correlation to rupture. Several hemodynamic indices and many biological patterns have been proposed that link hemodynamics to aneurysm formation, and evolution. These are well summarized by Singh *et al.*<sup>42</sup> Two hemodynamic indices, wall shear stress (WSS) and oscillatory shear index (OSI), have received particular attention due to their influence on endothelial cell behavior.<sup>6,40</sup>

Although studies from Rayz *et al.*,<sup>36</sup> Boussel *et al.*,<sup>1</sup> and Isoda *et al.*<sup>22</sup> showed that *in vivo* measurement of these quantities is possible using magnetic resonance, inherent limitations in the current technology impede its use, especially for smaller aneurysms, in large cohort studies.

In this context, computational fluid dynamics (CFD) can provide detailed predictions of hemodynamics using input parameters derived from medical imaging, blood sampling, and other patient information. CFD has been used by many groups to investigate possible correlations between hemodynamics and risk of rupture or growth of IAs. For convenience, the spatial extent of the computational domain is often limited to a restricted area around the aneurysm and specification of boundary conditions (BCs) at the interfaces with the rest of the cardiovascular network remains a pre-requisite to find a numerical solution. This issue is approached in different ways by different authors.

Some studies use patient-specific BCs based on measurements obtained using phase-contrast-MR (pc-MR) or transcranial Doppler (TCD) ultrasound, to record blood velocity, and applanation tonometry, to infer pressure. More recently Ferns and colleagues<sup>13</sup> have used a dual-sensor wire to measure *in vivo* pressure and blood flow velocity within intracranial vessels. These measurements are costly to perform, are currently rarely justifiable as part of the clinical routine and are inherently difficult to obtain for the small, intricate vessels of the cerebral vasculature hence, such studies often involve small cohorts and the results lack statistical significance.<sup>1,19,24</sup>

Larger cohort studies, in contrast, rely on inflow BCs based on measurements taken from healthy individuals, that are, in some cases<sup>8,23,29,35,44</sup> scaled in an attempt to achieve a more realistic mean WSS, and outflow BCs that arbitrarily assume the same pressure at all openings (zero pressure BCs). The assumptions associated with this approach may also lead to unrealistic results.

As detailed comparison with *in vivo* measurements is currently difficult, the validity of CFD tools in the

context of IA rupture-risk assessment relies upon the extent to which the correlations between hemodynamic predictions and rupture are statistically matched for a large cohort study. One of the important aims of @neurIST ([www.aneurist.org](http://www.aneurist.org)), a multidisciplinary EU project of which this study forms a part, is to establish these correlations by processing a large number of cases. The lack of patient-specific data for use at computational boundaries remains an important limiting factor in the project. This issue has been addressed by deriving a complete set of BCs for 3D CFD analysis from a 1D model of the circulatory system.<sup>37</sup>

This article analyses and compares the sensitivity of modeled hemodynamics within typical IAs to BCs derived using the 1D model, patient-specific pc-MR measurements, and other approaches described in the literature.

## MATERIALS AND METHODS

### *Study Design, Demographics, and Clinical Details*

The study was conducted as a co-operation between the Departments of Neurosurgery and Neuroradiology, Royal Hallamshire Hospital, and the Department of Cardiovascular Science, University of Sheffield, Sheffield, UK. A total of five patients diagnosed with IAs between Dec. 2006 and Jan. 2009, were identified retrospectively and followed prospectively upon appropriate ethical approval and patient consent. Table 1 shows the demographic constitution of the population along with the relevant aneurysm details. All IAs were side-wall saccular aneurysms with locations shown in Figs. 1 and 2.

### *X-ray Angiography Image Acquisition*

The medical images used for surface reconstruction were obtained using 3D rotational acquisition (3DRA) in a Philips® Integris™ Allura machine (Philips® Medical Systems, Best, The Netherlands), producing

**TABLE 1. Patient demographics and aneurysm radiological features.**

Aneurysm	Sex	Age	Side	Location	Rupture	Size (diam/neck) (mm)
1	M	44	Left	ICA	No	5/4.3
2	M	52	Left	MCA	No	11.1/4.3
3	F	50	Left	ICA	No	3.4/3.1
4	F	41	Right	MCA	Yes	4.4/3
5	F	51	Left	ICA	No	2.9/3.1

ICA, internal carotid artery; MCA, middle cerebral artery bifurcation.

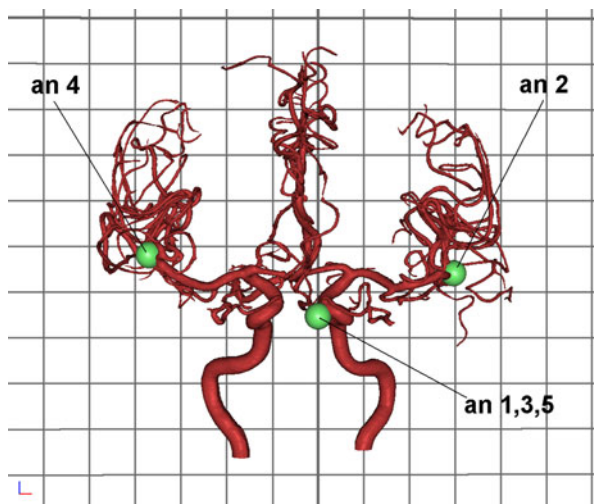


**FIGURE 1.** Locations of aneurysms 1–5 in typical cerebral vasculature (illustration generated using the @neurIST software).

100 images in 6 s, with 5 ms exposure per image. Voxel size in the reconstructed 3D images was 121 microns with reconstruction matrix of  $512 \times 512 \times 512$ .

#### *pc-MR Protocol*

All MR imaging was performed at high field strength (Achieva<sup>TM</sup> 3.0T, Philips<sup>®</sup> Medical Systems, Best, The Netherlands) using a standard eight-channel, radiofrequency receive-only head coil. The same radiographer imaged all patients to maximize the reproducibility of the overall acquisition technique.<sup>17</sup> A pre-designed protocol guided the radiographer through the desired measurement locations for subsequent application of CFD BCs. As afferent vasculature has an important influence on intra-aneurysmal hemodynamics,<sup>2,30,32,33</sup> proximal measurements were taken at a distance of approximately 10 parent vessel diameters from the aneurysm. Measurements in distal arteries were taken four diameters away from the IAs. To minimize patient discomfort, table-occupancy time was no greater than 1 h. Within this period it was difficult to ensure that all measurements were obtained for all patients. The tortuous nature of the vasculature also made slice selection perpendicular to the artery difficult to achieve. To maintain integrity in the final measurement data set, data was rejected if there was doubt about the placement of the measurement plane.

Locations of pc-MR measurements are reported Table 2. The manufacturer's proprietary post-data-acquisition software (Q-Flow<sup>TM</sup>, Philips<sup>®</sup> Medical Systems, Best, The Netherlands) was used to estimate volumetric flow rate (VFR) waveforms at each location.

#### *1D Circulation Model*

The model developed by Reymond *et al.*<sup>37</sup> was used to compute pressure and VFR waveforms at the desired interfaces with the 3D domains. The model solves the 1D form of the Navier–Stokes equation in a distributed model of the main human systemic arteries including the main arteries of the circle of Willis. It accounts for ventricular–vascular interaction and wall viscoelasticity, and it was recently validated through a comparison with *in vivo* flow measurements. Although the model could be personalized tuning input parameters such as heart rate, cardiac contractility, vessel elasticity, vessel geometry, and blood properties, in this study the model was used with the properties of a typical young individual as patient-specific data was not available for all patients. A typical analysis is solved in approximately 8 min.

#### *3D Models*

The @neurIST computational tool chain was used to reconstruct vessel and aneurysmal geometries, as described in Marzo *et al.*<sup>30</sup> The 3D transient Navier–Stokes equations were solved by using the finite-control-volume software, ANSYS<sup>®</sup>-CFX<sup>TM</sup>. Blood was assumed to be incompressible, with density  $\rho = 1060 \text{ kg m}^{-3}$ , and Newtonian, with viscosity  $\mu = 0.0035 \text{ Pa s}$ . BCs were applied using three different approaches, as reported in Table 2. *Method I* used pc-MR VFR measurements at the openings for which these could be measured, and 1D model pressure waveforms at every remaining interface. For aneurysm 1 and 5, measurements were available at all but one vessel opening. *Method II* used VFR and pressure waveforms from the 1D circulation model. *Method III* used the typical waveforms derived using the 1D model, where VFR curves were scaled to obtain a mean WSS of 1.5 Pa at inlets. For all velocity-based BCs a flat velocity profile was applied, in line with our recent finding.<sup>30</sup> Arterial walls were assumed to be rigid. The validity of this assumption has been tested in the context of IAs.<sup>11</sup> Tetrahedral elements were used to discretise the core of the computational domain, with three layers of prismatic elements at the wall to ensure accurate computation of the velocity gradients. Grid sizes with an average density of  $2000 \text{ el/mm}^3$  were used following a mesh dependency study in which WSS, pressure and velocity values, were monitored at several points within the aneurysm and parent vessel.<sup>35</sup> Figure 2 shows the meshes and BC types used in the analyses. To be independent of the initial numerical conditions hemodynamic data were extracted from the last cardiac cycle of a three-cycle analysis. Analyses were run

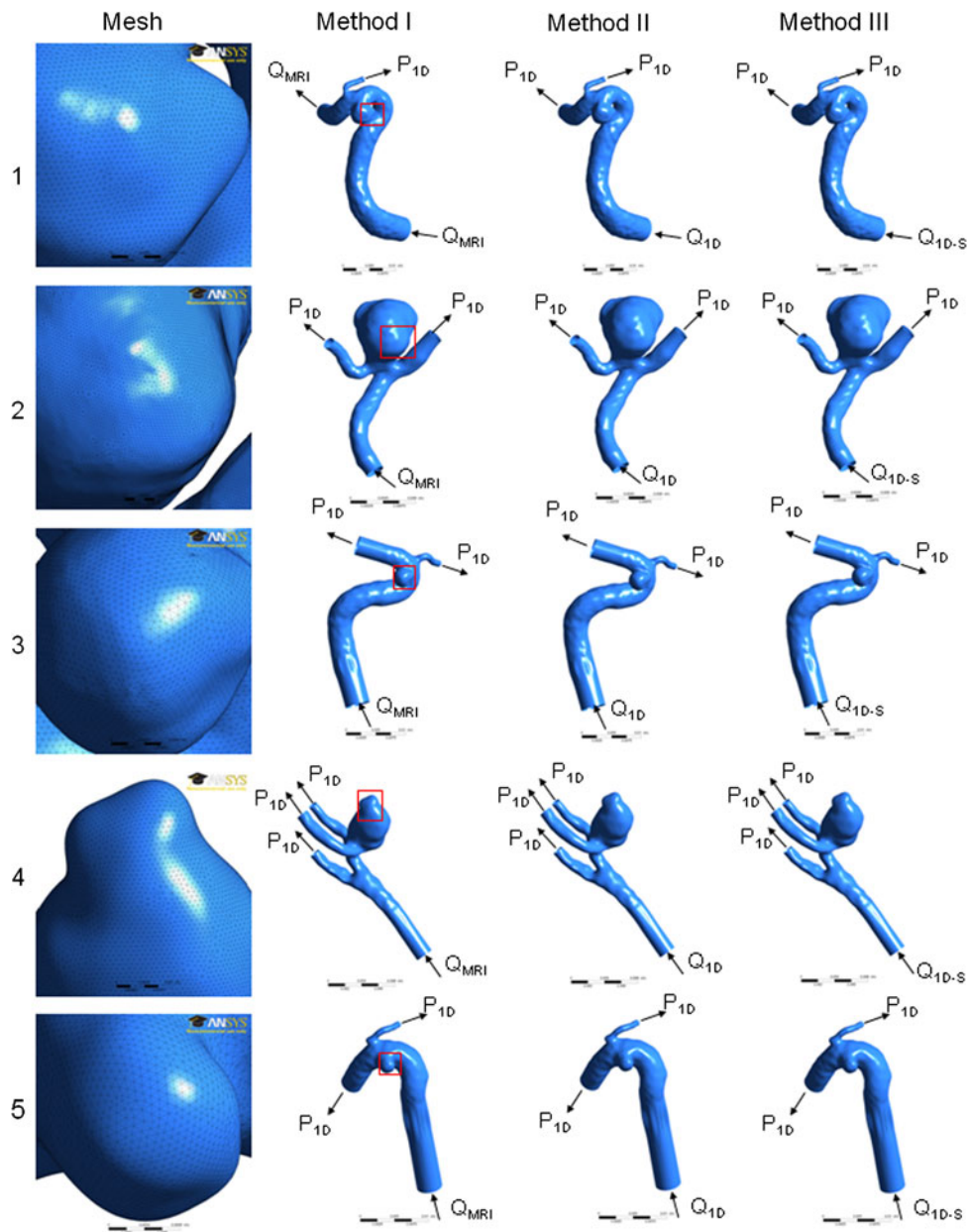


**FIGURE 2.** Mesh particulars and BC types used.  $Q_{MRI}$  is the velocity-based boundary condition from MRI patient-specific measurements,  $Q_{1D}$  is the velocity-based boundary condition from 1D model,  $Q_{1D-S}$  is the WSS-scaled velocity-based boundary condition from 1D model, and  $P_{1D}$  is the pressure boundary condition from 1D model.

in parallel using 30 cluster nodes (Xeon® 2.8 GHz, 2 GB RAM). The average time required to solve a complete three-cycle analysis was 5 h.

#### *Statistical Analysis*

Quantitative agreement between data obtained with the different BC methodologies was analyzed using boxplot diagrams.

## **RESULTS**

Hemodynamic variables were compared qualitatively and quantitatively for the BC methods analyzed.

#### *Qualitative Comparison*

Figure 3 shows contour distributions of WSS time-averaged along the cardiac cycle (tavWSS) at the wall of the IAs. For all methods, in aneurysms 1, 2, areas of



**TABLE 2. Boundary conditions location, type, and method.**

Aneurysm	BC location	Type	Method I	Method II	Method III
1	ICA proximal	Inlet	pc-MR/velocity	1D/velocity	1D/velocity scaled
	ICA distal	Outlet	pc-MR/velocity	1D/pressure	1D/pressure
	OphthA	Outlet	1D/pressure	1D/pressure	1D/pressure
2	MCA M1	Inlet	pc-MR/velocity	1D/velocity	1D/velocity scaled
	MCA M2 supr	Outlet	1D/pressure	1D/pressure	1D/pressure
	MCA M2 infr	Outlet	1D/pressure	1D/pressure	1D/pressure
3	ICA proximal	Inlet	pc-MR/velocity	1D/velocity	1D/velocity scaled
	ICA distal	Outlet	1D/pressure	1D/pressure	1D/pressure
	OphthA	Outlet	1D/pressure	1D/pressure	1D/pressure
4	MCA M1	Inlet	pc-MR/velocity	1D/velocity	1D/velocity scaled
	TempA	Outlet	1D/pressure	1D/pressure	1D/pressure
	MCA M2 supr	Outlet	1D/pressure	1D/pressure	1D/pressure
	MCA M2 infr	Outlet	1D/pressure	1D/pressure	1D/pressure
5	ICA proximal	Inlet	pc-MR/velocity	1D/velocity	1D/velocity scaled
	ICA distal	Outlet	pc-MR/velocity	1D/pressure	1D/pressure
	OphthA	Outlet	1D/pressure	1D/pressure	1D/pressure

ICA, internal carotid artery; OphthA, ophthalmic artery; MCA M1, middle cerebral artery; MCA M2 supr/infr, superior/inferior division of the middle cerebral artery; TempA, temporal artery.

relatively high WSS were concentrated around the aneurysmal neck and apex, while in aneurysm 5, an area of relatively high WSS is also present in the body. In aneurysms 3 and 4 only the neck is affected by high WSS, with the remainder of the aneurysmal wall exposed to lower WSS. For all aneurysms, areas of relatively low WSS were found in their bodies.

From a visual comparison of the contour plots, the most pronounced differences between method I (pc-MR) and method II (1D model) are in the distribution of  $\text{tavWSS}$  for aneurysms 1, 3, and 5, whereas aneurysms 2 and 4 showed closer agreement. In terms of qualitative differences between patient-specific and 1D model waveforms  $\text{tavWSS}$  values were underestimated when 1D-model BCs were applied, for all IAs except IA2.

Qualitative comparison of method I (pc-MR) and method III (WSS scaled) revealed larger differences than those observed when comparing methods I and II, except for aneurysm 1 where contour values of  $\text{tavWSS}$  are closer to the predictions of method I. For all IAs, the values of  $\text{tavWSS}$  obtained with method III are lower than those observed for method I.

Figure 4 shows contours of normalized values of  $\text{tavWSS}$  ( $\text{ntavWSS}$ ). Normalization was achieved by dividing the absolute values of  $\text{tavWSS}$  by the spatial average of  $\text{tavWSS}$  at the aneurysmal wall. Interestingly, for all methods, there is similarity in the overall distribution of areas of proportionally higher, or lower, WSS.

Figure 5 shows contour distributions of OSI on the aneurysmal surface. Although small differences can be observed, the OSI patterns are very similar.

As expected, areas of elevated OSI tend to be associated with low  $\text{tavWSS}$ . OSI values obtained with method II look closer to the pc-MR-based values, than those obtained using method III.

#### *Quantitative Comparison*

Figure 6 shows the boxplots diagrams of the percentage differences between method I and method II (top boxplot) and method I and method III (bottom boxplot) for selected indices computed within the aneurysmal sac, namely; maximum OSI (mOSI), normalized maximum value of time-average WSS ( $\text{nmtavWSS}$ ), maximum time-average WSS ( $\text{mtavWSS}$ ), maximum time-average velocity ( $\text{mtavU}$ ) and spatial and time-average velocity ( $\text{stavU}$ ). The percentage error was calculated from  $(\text{index\_value}_{\text{method I}} - \text{index\_value}_{\text{method X}})100/\text{index\_value}_{\text{method I}}$ . As previously observed qualitatively, comparisons show that the smallest discrepancies are observed in the values of mOSI and  $\text{nmtavWSS}$  (median value 17.5–23.5% for mOSI and 11–20.5% for  $\text{nmtavWSS}$ ). The hemodynamic index showing highest discrepancies is  $\text{mtavWSS}$  with median values of 46% for method I versus II and 69% for method I versus III.

When considering the cross-comparison of methods II (1D model) and III (WSS scaled) with method I (pc-MR) (which is assumed to be the gold standard), the largest discrepancies are observed for the comparison between methods I and III. If we consider only the median values of each index we observe that, for method I, all indices perform better than their counterpart in method III.

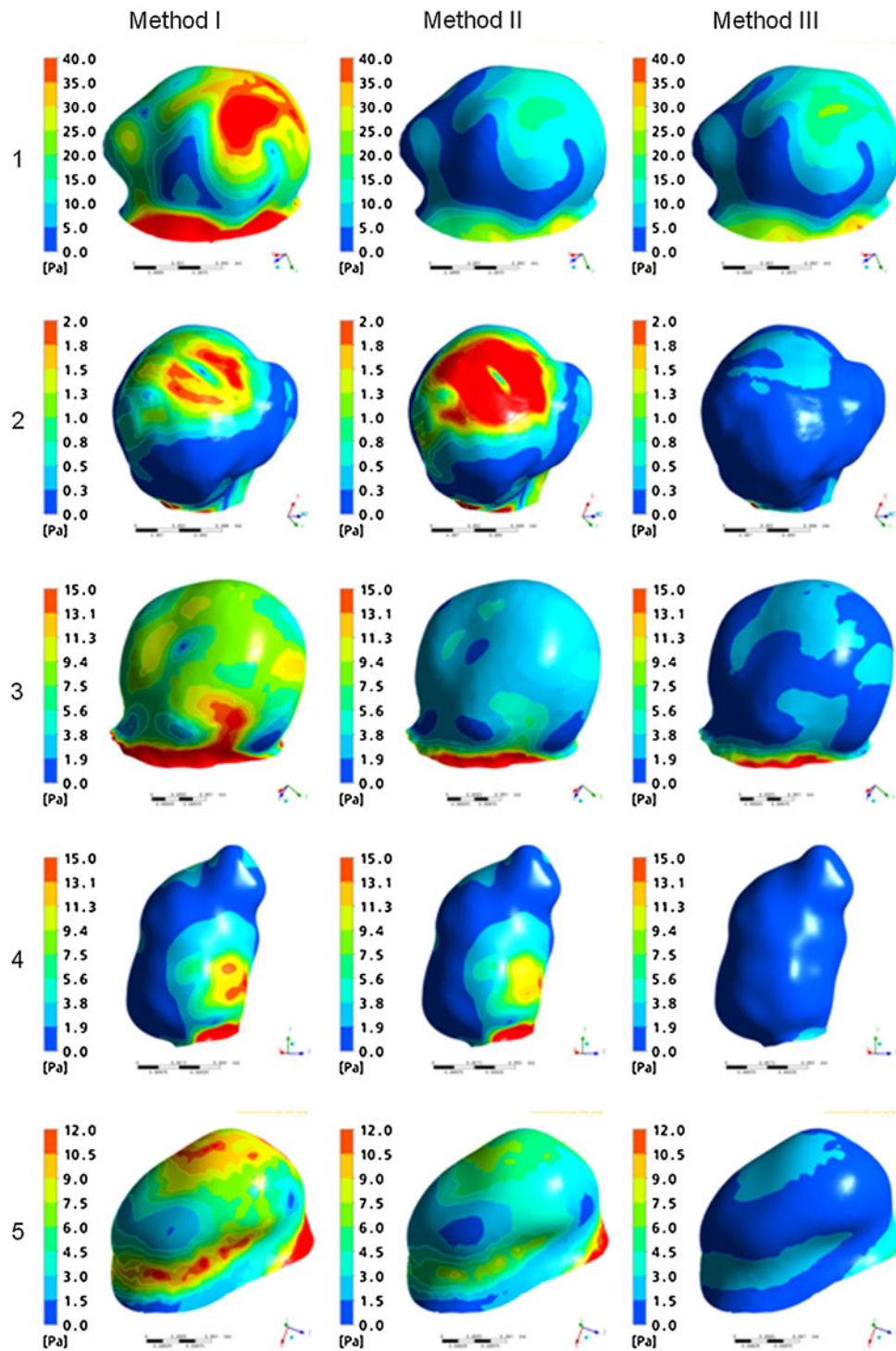


FIGURE 3. Contour plots of  $\text{tavWSS}$  for method I (pc-MR), method II (1D model), and method III (WSS scaled).

## DISCUSSION

In creating a computational model to predict the hemodynamics in an IA, assumptions are often made that can adversely affect the numerical results. One of the most important areas where assumptions are

required is the application of BCs. Several authors have demonstrated the significant influence of BCs on computed hemodynamic indices.<sup>9,19,44</sup>

Depending on the method of derivation, BCs can be broadly divided into two categories; those that are patient-specific and those that are non-patient-specific.

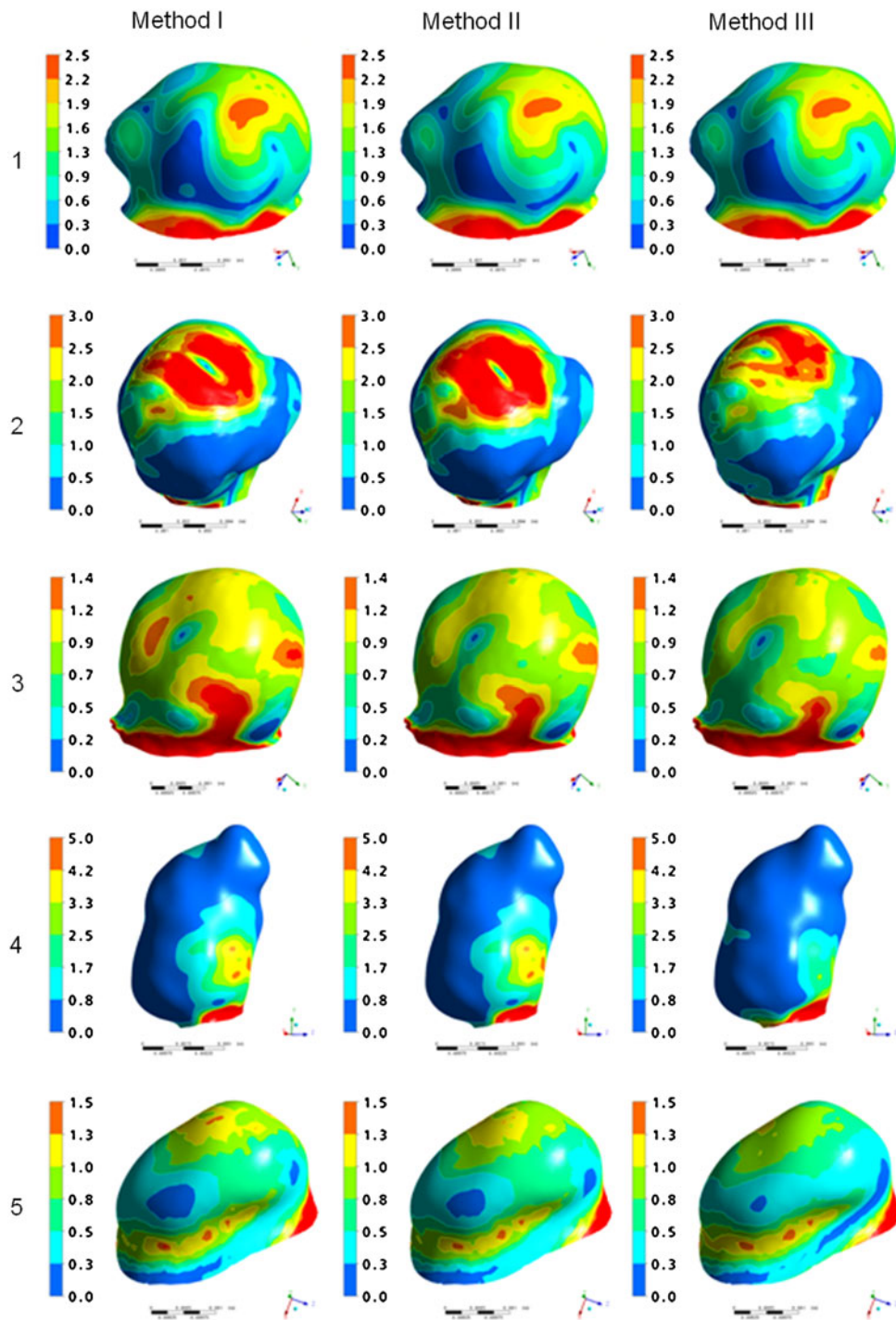


**FIGURE 4.** Contour plots of normalized values of  $\text{tavWSS}$  for method I (pc-MR), method II (1D model), and method III (WSS scaled).

#### *Patient-Specific BC's*

Patient-specific BCs are understandably considered the “gold standard.”<sup>9,19,44</sup> Unfortunately, these are rarely available. Of 24 articles reviewed for this study (Table 3), only 6 (25%) used patient-specific BCs.<sup>1,19,24</sup> pc-MR was the most common modality (5 out of 6)

used to obtain patient-specific measurements, with TCD used by one author.<sup>19</sup> Most authors (5 out of 6), applied these measurements only at inlets. Only one group, Jou and colleagues,<sup>25</sup> used patient-specific pc-MR measurements at both inlets and outlet when analyzing a basilar artery fusiform aneurysm. Thus,



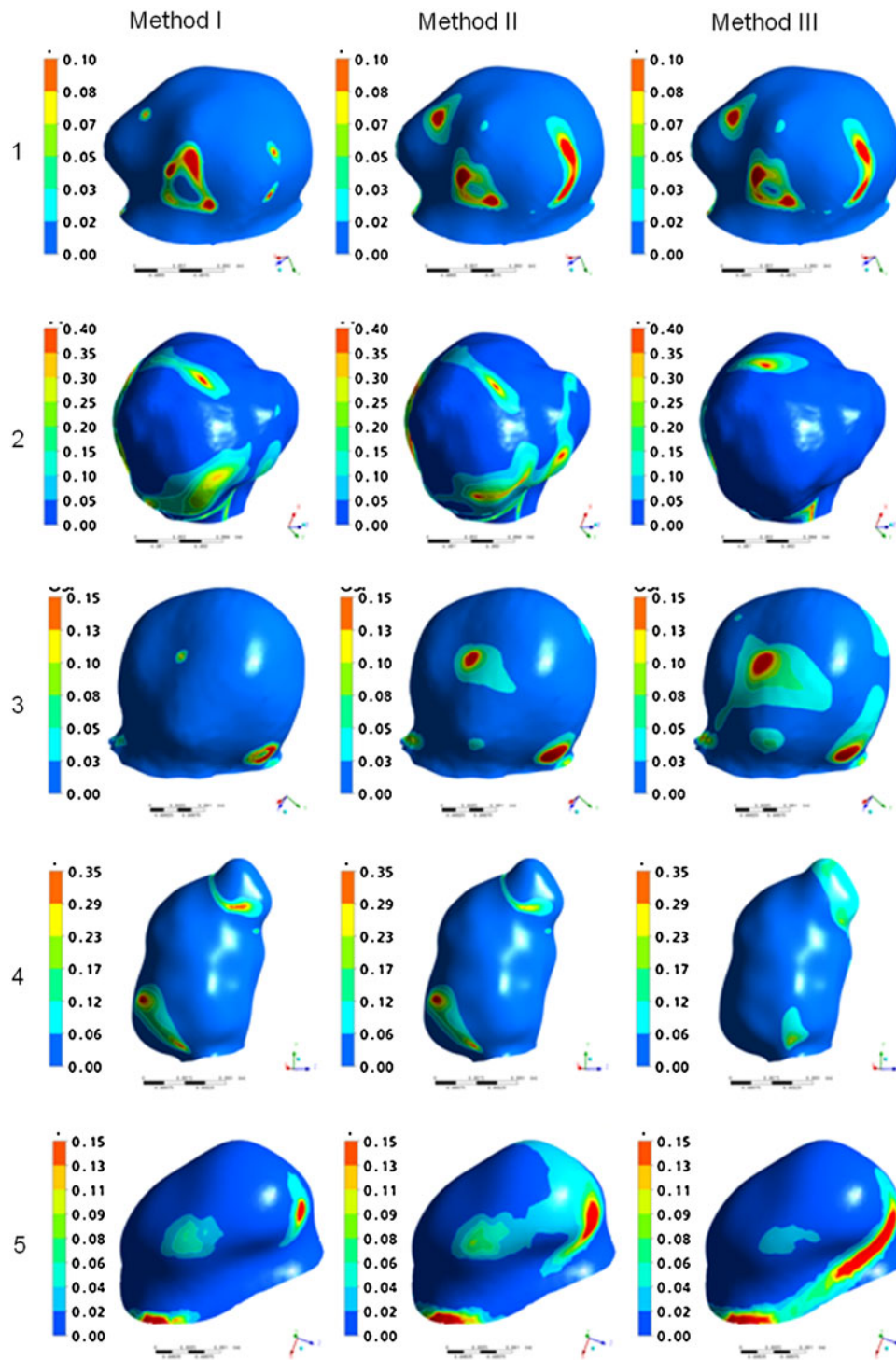
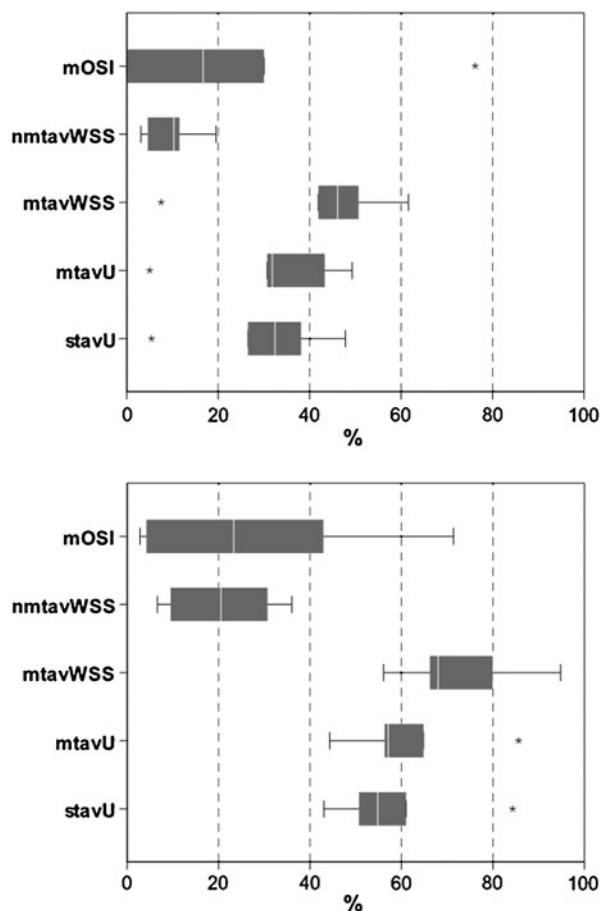


FIGURE 5. Contour plots of OSI for method I (pc-MR), method II (1D model), and method III (WSS scaled).

even when patient-specific measurements can be justified in a busy clinical setting, technical difficulties may compromise their application at all openings, further limiting their use in establishing statistical correlations with rupture. In fact, a major constraint when adopting patient-specific BCs is that due to current

restrictions in obtaining these measurements, they have not been applied in large cohort studies, thus compromising the possibility of using CFD to find significant statistical correlations between hemodynamics and aneurysmal evolution (initiation, growth, and rupture). In the current review, the mean cohort size





**FIGURE 6.** Boxplots showing the distribution percentage differences between method I and II (top) and method I and III (bottom). Asterisks denote outliers above or below 1.5 times the inter-quartile range.

for the patient-specific BC group was significantly smaller, i.e. 3 (range 1–7) compared to 9.5 (range 1–62) when non-patient-specific BCs were used. Another important aspect one has to consider: there may be significant diurnal variation in values for an individual associated with stress or anxiety,<sup>12,27</sup> physical exertion,<sup>16,21</sup> and other day-to-day activities.<sup>18</sup> It can be argued that patient-specific BCs, invariably measured with a patient lying quietly in a scanner surrounded by an artificial environment or stressed by the overall clinical experience (e.g., white-coat hypertension), might not represent the normal day-to-day physiology for that individual, and thus might not represent exactly the type of BCs needed for statistical associations. Gonzalez-Alonso *et al.*<sup>16</sup> recorded a population-average flow rate variation as high as 1 mL/s at the level of middle cerebral artery level between rest and exercise.

Another important aspect is the error associated with blood flow measurement. For quantitative MR angiography average measurement errors have

been reported to be as high as 7.6% for pulsatile flow.<sup>45</sup>

#### *Non-Patient-Specific BC*

In absence of patient-specific BCs many investigators use typical or modeled BCs. Out of 24 papers, 18 (75%) used this approach. Waveforms are usually obtained from population-averaged measurements taken on healthy volunteers.<sup>14,43</sup> While the use of such waveforms remains the most popular method of BC application (17 out of 18 non-patient-specific BCs in our review), the method carries important limitations. First, as these measurements are taken in a healthy population, they may not be representative of patient waveforms. This is illustrated in Fig. 7, where waveforms from a healthy volunteer show differences both in shape and values, when compared with those for patients 1, 3, and 5.

Second, these waveforms represent average values of pressure and velocity across the population, and lack adaptability in terms of location and vessel geometrical properties. In an attempt to address these issues and make these typical waveforms more patient-specific, Cebral and colleagues<sup>7</sup> suggested “scaling” the inflow rates to the inflow boundary area to keep the WSS within a “physiological” range (around 1.5 Pa). The same approach has been adopted by other scientists.<sup>23,31,35</sup> Although Cebral and co-workers found an important flow-area correlation based on experimental evidence at some specific vessel locations, their approach can be very sensitive to the boundary location along the vessel, due to diameter variations along the vessel, and to segmentation error and image modality. This approach may be appropriate for a typical healthy individual but, as reported by many authors in the field, it is predominantly atypical variations in hemodynamics (e.g., WSS) that are believed to influence the etiopathogenesis of IAs.<sup>38,40</sup> Cheng *et al.*<sup>10</sup> challenged this hypothesis in their recent review, which showed large variations of average WSS (range 0.2–1.6 Pa). Atypical values of WSS have been associated with other conditions such as maladaptive growth, congenital malformations, patent ductus arteriosus, and atherosclerosis.

Quarteroni and collaborators pioneered the concept of using lumped and 1D-circulation models in an attempt to provide realistic BCs to 3D models.<sup>15,28,34</sup> More recently in 2009, we<sup>30</sup> introduced the use of a 1D-circulation model to derive BCs while studying hemodynamics within IAs. This model is used in the current study. The parameters of the 1D model used are relative to a healthy typical individual, an approach exposed to the limitations mentioned above for typical “healthy” waveforms. Indeed, this might

**TABLE 3. A comprehensive review showing the methods adapted by different authors while applying BCs.**

No.	Author/references	Cohort size (IAs)	IA location (s)	BC type/location	BC source (method)
1	Steinman <i>et al.</i> <sup>43</sup>	1	Terminal ICA	Inlet/ICA Outlets/MCA, ACA	Healthy subjects (pc-MR) Traction free
2	Chatziprodromou <i>et al.</i> <sup>9</sup>	2	Supraclinoid ICA	Inlets/ICA Outlets/ICA	Idealized Traction free
3	Jou <i>et al.</i> <sup>24</sup>	1	BA (fusiform)	Inlets/VA Outlet/BA	Patient-specific (pc-MR) Patient-specific (pc-MR)
4	Hassan <i>et al.</i> <sup>19</sup>	1	Vertebro-basilar	Inlet/VA Outlet/BA	Patient-specific (TCD) Traction free
5	Shojima <i>et al.</i> <sup>40</sup>	20	MCA	Inlets/MCA-M1 Outlets/MCA-M2	Healthy subjects (TCD) Traction free
6	Cebral <i>et al.</i> <sup>6</sup>	62	ICA (22), MCA (14), Pcom (13), ACA (1), Post (9), (3 NA)	Inlets/ICA, MCA, ACA, BA Outlets/NA	Healthy subjects (pc-MR) NA
7	Jou <i>et al.</i> <sup>25</sup>	2	BA (fusiform)	Inlets/VA Outlets/PCA	Patient-specific (pc-MR) NA
8	Shojima <i>et al.</i> <sup>41</sup>	29	ICA (14), MCA (14), ACA (1)	Inlets/ICA Outlets/ICA, MCA	Healthy subjects (TCD) Traction free
9	Cebral <i>et al.</i> <sup>5</sup>	4	ICA (2), SCA (1), Pcom (1)	Inlets/NA Outlets/NA	Healthy subjects (pc-MR) Traction free
10	Karmonik <i>et al.</i> <sup>26</sup>	3	BA (top)	Inlets/BA, VA Outlet	Healthy subjects (pc-MR) NA
11	Castro <i>et al.</i> <sup>2</sup>	4	Pcom (1), Acom (1), MCA (2)	Inlets/NA Outlets/NA	Healthy subjects (pc-MR) Traction free
12	Castro <i>et al.</i> <sup>4</sup>	7	Acom (1), BA (1), ICA (2), MCA (1), SCA (1), PCA (1)	Inlets/NA Outlets/NA	Healthy subjects (pc-MR) Traction free
13	Castro <i>et al.</i> <sup>3</sup>	2	Acom	Inlets/ICA Outlets/NA	Healthy subjects (pc-MR) Traction free
14	Mantha <i>et al.</i> <sup>29</sup>	3	ICA	Inlets/NA Outlets/NA	Healthy subjects (scaled) NA
15	Venugopal <i>et al.</i> <sup>44</sup>	1	Acom	Inlets/A1 Outlets/A2	Healthy subjects (scaled) Zero pressure
16	Boussel <i>et al.</i> <sup>1</sup>	7	BA (3), ICA (3), MCA (3)	Inlets/NA Outlets/NA	Patient-specific (pc-MR) NA
17	Mitsos <i>et al.</i> <sup>31</sup>	1	Acom	Inlet/NA Outlet/NA	Healthy subjects (LDV) Traction free
18	Rayz <i>et al.</i> <sup>36</sup>	4	BA	Inlets/VA Outlets/PCA	Patient specific (pc-MR) Traction free
19	Radaelli <i>et al.</i> <sup>35</sup>	1	ICA	Inlet/ICA-proximal Outlet/ICA-distal	Healthy subjects (scaled) Traction free
20	Rayz <i>et al.</i> <sup>36</sup>	3	BA	Inlet/VA Outlet/PCA	Patient-specific (pc-MR) Likely traction free
21	Shimogonya <i>et al.</i> <sup>39</sup>	1	ICA	Inlet/ICA-proximal Outlet/ICA-distal	Healthy subjects waveforms Traction free
22	Jou <i>et al.</i> <sup>23</sup>	26	ICA-clinoidal	Inlets/ICA Outlet/NA	Healthy subjects (scaled) NA
23	Marzo <i>et al.</i> <sup>30</sup>	3	BA, ICA	Inlet/BA, ICA-proximal Outlet/BA, ICA-distal	Computed (1-D model) Traction free
24	Cebral <i>et al.</i> <sup>8</sup>	1	BA (top)	Inlet/mid-BA Outlets/PCA	Healthy subjects (scaled) Traction free

BCs, boundary conditions; PC-MR, phase contrast magnetic resonance angiography; TCD, trans-cranial Doppler's ultrasound; LDV, laser Doppler velocimetry; ICA, internal carotid artery; ACA, anterior cerebral artery; Acom, anterior communicating artery; MCA, middle cerebral artery; Pcom, posterior communicating artery; SCA, superior cerebellar artery; BA, basilar artery; VA, vertebral artery; Post, posterior circulation.

explain, in part, the quantitative discrepancies observed. The use of a 1D model, however, has the advantage of allowing flexibility in the location of the model boundaries and, more importantly, has the potential for adaptation to patient-specific parameters,

when available, to obtain more representative values at the boundaries. The comparison in Fig. 6 (top) shows important differences between 1D model and pc-MR data ranging from a minimum median value of 11% (OSI) to a maximum of 46% (mtavWSS).

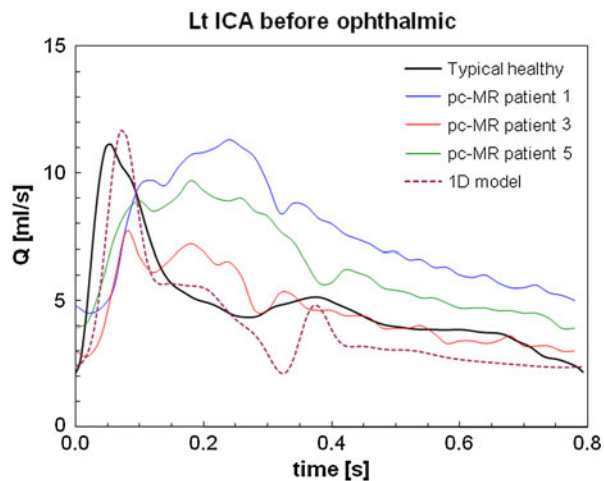


**FIGURE 7.** VFR waveforms for a typical healthy individual and aneurysm patients included in this study, measured using pc-MR at internal carotid level. Typical waveform was taken from Radaelli *et al.*<sup>35</sup>

**TABLE 4.** Time-average volumetric flow rates and inlet radii for the five aneurysms.

	$Q_{av-MR}$ (mL/s)	$Q_{av-1D}$ (mL/s)	$Q_{av-wss}$ (mL/s)	$r_{pt}$ (mm)	$r_{1D}$ (mm) <sup>a</sup>
Aneu-1	7.53	3.95	4.31	2.3	2.1–2.6
Aneu-2	1.46	1.90	0.74	1.3	1.4–1.5
Aneu-3	6.36	3.94	3.11	2.1	2.1–2.6
Aneu-4	2.00	1.91	0.42	1.1	1.4–1.5
Aneu-5	5.44	3.95	2.21	1.9	2.1–2.6

Aneu, aneurysm; Pt, patient;  $Q_{av-MR}$ , average flow measured using pc-MR;  $Q_{av-1D}$ , average flow predicted by 1D-model;  $Q_{av-WSS}$ , average flow predicted by 1D-model scaled to obtain  $wss = 1.5$  Pa at boundary;  $r_{pt}$ , radius of the vessel as measured in the patient;  $r_{1D}$ , average radius of the vessel used in 1D-model.

<sup>a</sup>Min and max radii in 1D model vessel where BCs was originated.

These discrepancies, however, are determined by differences in flow rates between the 1D model and patient-specific waveforms, which are of the same order of magnitude to physiological variations reported by Gonzalez-Alonso *et al.*<sup>16</sup>, see Table 4. While there are quantitative differences in hemodynamic indices obtained by the different methods, comparisons using normalized data showed that the distribution of WSS remains unchanged. This confirms once again the significance of geometry in determining the hemodynamic development within the aneurysm,<sup>5,30</sup> but also some degree of linearity of the results with respect to the flow within the aneurysm. Table 5 shows information on geometry and flow immediately proximal to the aneurysm sac for all three methods considered.  $Re$  values show a certain degree of linearity with respect to the absolute values reported in Fig. 3.

Comparisons of OSI values showed good agreement between the three methods. This is to be expected

**TABLE 5.** Reynolds numbers of flow approaching aneurysm, aneurysm aspect ratios, and vessel radii.

Aneurysm	$Re$ I	$Re$ II	$Re$ III	Surface ratio	$r_{prox}$ (mm)
1	551	285	311	4.7	1.8
2	140	228	89	20.1	1.3
3	343	223	176	5.6	2.1
4	155	184	138	15.5	0.9
5	434	298	152	2.5	1.9

$Re$  I–II–III, Reynolds numbers of flow approaching aneurysm for pc-MRI (I), 1D model (II), and WSS-scaled (III) boundary conditions methods measured at end diastole; Surface ratio, aneurysm surface area over neck surface area;  $r_{prox}$ , vessel radius proximal to aneurysm.

as OSI, in its definition, uses the normalization of local WSS.

Although blood is a non-Newtonian fluid, in this study we made the assumption of constant viscosity. This is a valid assumption in the context of a study whose aim is to evaluate the influence of BCs on intra-aneurysmal flow. In this respect, the use of a non-Newtonian model would have negligible influence on our findings as the same rheology model would be consistently used to study the influence of BCs. Also, Cebal *et al.*<sup>5</sup> showed that the sensitivity of hemodynamic predictions to different rheology models is negligible in the context of aneurysmal hemodynamics.

The current study would benefit from a larger aneurysm cohort (although this would, of course, be subject to clinical limitations), and from a wider range of aneurysm locations (for example, aneurysm of the anterior communicating artery (AComMA) or basilar artery), which were not available in this study.

### Summary

Whereas we can easily extract information about aneurysm and vessel geometry, measurements of blood flow to be used as BCs in numerical predictions are more difficult to determine. As hemodynamic factors are believed to be important in the aneurysm natural history, we investigated the variability of certain hemodynamic parameters with BCs. In this preliminary study differences were found between results obtained with patient-specific and modeled BCs. These are attributable to underlying differences in the  $Re$  of the flow approaching the aneurysms. In fact, discrepancies were significantly reduced when considering normalized indices, suggesting a certain degree of linearity in the results and the important role played by geometry in intraneurysmal hemodynamics. It is likely that in the future patient-specific BCs will be provided as a part of routine clinical procedure. Until then, affirmation of CFD will be based on finding statistical correlations using non-patient-specific BCs. The results



of this study show that modeled BCs allow realistic predictions of IA hemodynamics and offer a viable means for finding correlations with rupture in large cohort studies.

### ACKNOWLEDGMENTS

The @neurIST project is funded by the European Commission, VI Framework Programme, Priority 2, Information Society Technologies (Oxfordshire Research Ethics Committee—A Study Number: 07/Q1604/53).

### REFERENCES

- <sup>1</sup>Boussel, L., V. Rayz, *et al.* Aneurysm growth occurs at region of low wall shear stress: patient-specific correlation of hemodynamics and growth in a longitudinal study. *Stroke* 39(11):2997–3002, 2008.
- <sup>2</sup>Castro, M. A., C. M. Putman, *et al.* Computational fluid dynamics modeling of intracranial aneurysms: effects of parent artery segmentation on intra-aneurysmal hemodynamics. *AJNR Am. J. Neuroradiol.* 27(8):1703–1709, 2006.
- <sup>3</sup>Castro, M. A., C. M. Putman, *et al.* Patient-specific computational fluid dynamics modeling of anterior communicating artery aneurysms: a study of the sensitivity of intra-aneurysmal flow patterns to flow conditions in the carotid arteries. *AJNR Am. J. Neuroradiol.* 27(10):2061–2068, 2006.
- <sup>4</sup>Castro, M. A., C. M. Putman, *et al.* Patient-specific computational modeling of cerebral aneurysms with multiple avenues of flow from 3D rotational angiography images. *Acad. Radiol.* 13(7):811–821, 2006.
- <sup>5</sup>Cebral, J. R., M. A. Castro, *et al.* Efficient pipeline for image-based patient-specific analysis of cerebral aneurysm hemodynamics: technique and sensitivity. *IEEE Trans. Med. Imaging* 24(4):457–467, 2005.
- <sup>6</sup>Cebral, J. R., M. A. Castro, *et al.* Characterization of cerebral aneurysms for assessing risk of rupture by using patient-specific computational hemodynamics models. *AJNR Am. J. Neuroradiol.* 26(10):2550–2559, 2005.
- <sup>7</sup>Cebral, J. R., M. A. Castro, *et al.* Flow–area relationship in internal carotid and vertebral arteries. *Physiol. Meas.* 29(5):585–594, 2008.
- <sup>8</sup>Cebral, J. R., S. Hendrickson, *et al.* Hemodynamics in a lethal basilar artery aneurysm just before its rupture. *AJNR Am. J. Neuroradiol.* 30(1):95–98, 2009.
- <sup>9</sup>Chatziprodromou, I., V. D. Butty, *et al.* Pulsatile blood flow in anatomically accurate vessels with multiple aneurysms: a medical intervention planning application of computational haemodynamics. *Flow Turbul. Combust.* 71:333–346, 2003.
- <sup>10</sup>Cheng, C., F. Helderma, *et al.* Large variations in absolute wall shear stress levels within one species and between species. *Atherosclerosis* 195(2):225–235, 2007.
- <sup>11</sup>Dempere-Marco, L., E. Oubel, *et al.* CFD analysis incorporating the influence of wall motion: application to intracranial aneurysms. *Med. Image Comput. Comput. Assist. Interv.* 9(Pt 2):438–445, 2006.
- <sup>12</sup>Fedorov, B. M., T. V. Sebekina, *et al.* [Stress and blood circulation in man]. *Kosm. Biol. Aviakosm. Med.* 24(3):35–40, 1990.
- <sup>13</sup>Ferns, S. P., J. J. Schneiders, *et al.* Intracranial blood-flow velocity and pressure measurements using an intra-arterial dual-sensor guidewire. *AJNR Am. J. Neuroradiol.* 31(2):324–326, 2010.
- <sup>14</sup>Ford, M. D., H. N. Nikolov, *et al.* PIV-measured versus CFD-predicted flow dynamics in anatomically realistic cerebral aneurysm models. *J. Biomech. Eng.* 130(2):021015, 2008.
- <sup>15</sup>Formaggia, L., J. F. Gerbeau, *et al.* On the coupling of 3d and 1d Navier–Stokes equations for flow problems in compliant vessels. *Comput. Methods Appl. Mech. Eng.* 191:561–582, 2001.
- <sup>16</sup>Gonzalez-Alonso, J., M. K. Dalsgaard, *et al.* Brain and central haemodynamics and oxygenation during maximal exercise in humans. *J. Physiol* 557(Pt 1):331–342, 2004.
- <sup>17</sup>Gwilliam, M. N., N. Hoggard, *et al.* MR derived volumetric flow rate waveforms at locations within the common carotid, internal carotid, and basilar arteries. *J. Cereb. Blood Flow Metab.* 29(12):1975–1982, 2009.
- <sup>18</sup>Hajjar, I., M. Selim, *et al.* The relationship between nighttime dipping in blood pressure and cerebral hemodynamics in nonstroke patients. *J. Clin. Hypertens. (Greenwich)* 9(12):929–936, 2007.
- <sup>19</sup>Hassan, T., M. Ezura, *et al.* Computational simulation of therapeutic parent artery occlusion to treat giant vertebrobasilar aneurysm. *AJNR Am. J. Neuroradiol.* 25(1):63–68, 2004.
- <sup>20</sup>Hop, J. W., G. J. Rinkel, *et al.* Case-fatality rates and functional outcome after subarachnoid hemorrhage: a systematic review. *Stroke* 28(3):660–664, 1997.
- <sup>21</sup>Ide, K., and N. H. Secher. Cerebral blood flow and metabolism during exercise. *Prog. Neurobiol.* 61(4):397–414, 2000.
- <sup>22</sup>Isoda, H., Y. Ohkura, *et al.* In vivo hemodynamic analysis of intracranial aneurysms obtained by magnetic resonance fluid dynamics (MRFD) based on time-resolved three-dimensional phase-contrast MRI. *Neuroradiology* 52(10):921–928, 2010.
- <sup>23</sup>Jou, L. D., D. H. Lee, *et al.* Wall shear stress on ruptured and unruptured intracranial aneurysms at the internal carotid artery. *AJNR Am. J. Neuroradiol.* 29(9):1761–1767, 2008.
- <sup>24</sup>Jou, L. D., C. M. Quick, *et al.* Computational approach to quantifying hemodynamic forces in giant cerebral aneurysms. *AJNR Am. J. Neuroradiol.* 24(9):1804–1810, 2003.
- <sup>25</sup>Jou, L. D., G. Wong, *et al.* Correlation between luminal geometry changes and hemodynamics in fusiform intracranial aneurysms. *AJNR Am. J. Neuroradiol.* 26(9):2357–2363, 2005.
- <sup>26</sup>Karmonik, C., G. Benndorf, *et al.* Wall shear stress variations in basilar tip aneurysms investigated with computational fluid dynamics. *Conf. Proc. IEEE Eng. Med. Biol. Soc.* 1:3214–3217, 2006.
- <sup>27</sup>Kulikov, V. P., V. N. Grechishnikov, *et al.* [Response of cerebral hemodynamics to combined stress impacts]. *Patol. Fiziol. Eksp. Ter.* 1:7–9, 2005.
- <sup>28</sup>Lagana, K., G. Dubini, *et al.* Multiscale modelling as a tool to prescribe realistic boundary conditions for the study of surgical procedures. *Biorheology* 39(3–4):359–364, 2002.

- <sup>29</sup>Mantha, A., C. Karmonik, *et al.* Hemodynamics in a cerebral artery before and after the formation of an aneurysm. *AJNR Am. J. Neuroradiol.* 27(5):1113–1118, 2006.
- <sup>30</sup>Marzo, A., P. Singh, *et al.* Influence of inlet boundary conditions on the local haemodynamics of intracranial aneurysms. *Comput. Methods Biomech. Biomed. Eng.* 12(4): 431–444, 2009.
- <sup>31</sup>Mitsos, A. P., N. M. Kakalis, *et al.* Haemodynamic simulation of aneurysm coiling in an anatomically accurate computational fluid dynamics model: technical note. *Neuroradiology* 50(4):341–347, 2008.
- <sup>32</sup>Moyle, K. R., L. Antiga, *et al.* Inlet conditions for image-based CFD models of the carotid bifurcation: is it reasonable to assume fully developed flow? *J. Biomech. Eng.* 128(3):371–379, 2006.
- <sup>33</sup>Oshima, M., H. Sakai, *et al.* Modelling of inflow boundary conditions for image-based simulation of cerebrovascular flow. *Int. J. Numer. Methods Fluids* 47:603–617, 2005.
- <sup>34</sup>Quarteroni, A., and L. Formaggia. Mathematical modeling and numerical simulation of the cardiovascular system. In: *Handbook of Numerical Analysis*, Vol. 12, edited by P. G. Ciarlet, and J. L. Lions. Amsterdam: Elsevier, 2004, pp. 3–127.
- <sup>35</sup>Radaelli, A. G., L. Augsburger, *et al.* Reproducibility of haemodynamical simulations in a subject-specific stented aneurysm model—a report on the Virtual Intracranial Stenting Challenge 2007. *J. Biomech.* 41(10):2069–2081, 2008.
- <sup>36</sup>Rayz, V. L., L. Bussel, *et al.* Numerical simulations of flow in cerebral aneurysms: comparison of CFD results and in vivo MRI measurements. *J. Biomech. Eng.* 130(5): 051011, 2008.
- <sup>37</sup>Reymond, P., F. Merenda, *et al.* Validation of a one-dimensional model of the systemic arterial tree. *Am. J. Physiol. Heart Circ. Physiol.* 297(1):H208–H222, 2009.
- <sup>38</sup>Sekhar, L. N., and R. C. Heros. Origin, growth, and rupture of saccular aneurysms: a review. *Neurosurgery* 8(2): 248–260, 1981.
- <sup>39</sup>Shimogonya, Y., T. Ishikawa, *et al.* Can temporal fluctuation in spatial wall shear stress gradient initiate a cerebral aneurysm? A proposed novel hemodynamic index, the gradient oscillatory number (GON). *J. Biomech.* 42(4): 550–554, 2009.
- <sup>40</sup>Shojima, M., M. Oshima, *et al.* Magnitude and role of wall shear stress on cerebral aneurysm: computational fluid dynamic study of 20 middle cerebral artery aneurysms. *Stroke* 35(11):2500–2505, 2004.
- <sup>41</sup>Shojima, M., M. Oshima, *et al.* Role of the bloodstream impacting force and the local pressure elevation in the rupture of cerebral aneurysms. *Stroke* 36(9):1933–1938, 2005.
- <sup>42</sup>Singh, P. K., A. Marzo, *et al.* Effects of heparin on the hemodynamic characteristics of intracranial aneurysms. *J. Neuroradiol.* Apr 5.
- <sup>43</sup>Steinman, D. A., J. S. Milner, *et al.* Image-based computational simulation of flow dynamics in a giant intracranial aneurysm. *AJNR Am. J. Neuroradiol.* 24(4):559–566, 2003.
- <sup>44</sup>Venugopal, P., D. Valentino, *et al.* Sensitivity of patient-specific numerical simulation of cerebral aneurysm hemodynamics to inflow boundary conditions. *J. Neurosurg.* 106(6):1051–1060, 2007.
- <sup>45</sup>Zhao, M., S. Amin-Hanjani, *et al.* Regional cerebral blood flow using quantitative MR angiography. *AJNR Am. J. Neuroradiol.* 28(8):1470–1473, 2007.